Author Manuscript

Author Manuscript

Author Manuscript

Author Manuscript

HHS Public Access

Author manuscript

Cell. Author manuscript; available in PMC 2016 January 25.

Published in final edited form as:

Cell. 2014 June 5; 157(6): 1405–1415. doi:10.1016/j.cell.2014.03.061.

Molecular basis for age-dependent microtubule acetylation by tubulin acetyltransferase

Agnieszka Szyk[1,†], **Alexandra M. Deaconescu**[2,†,‡], **Jeffrey Spector**[1,†], **Benjamin Goodman**[1], **Max L. Valenstein**[1], **Natasza E. Ziolkowska**[1], **Vasilisa Kormendi**[1], **Nikolaus Grigorieff**[2], and **Antonina Roll-Mecak**[1,3,*]

[1]Cell Biology and Biophysics Unit, Porter Neuroscience Research Center, National Institute of Neurological Disorders and Stroke, Bethesda, MD 20892, U.S.A.

[2]Janelia Farm Research Campus, Howard Hughes Medical Institute, Ashburn, VA 20147, U.S.A.

[3]National Heart, Lung and Blood Institute, Bethesda, MD 20892, U.S.A.

Abstract

Acetylation of α-tubulin Lys40 by tubulin acetyltransferase (TAT) is the only known posttranslational modification in the microtubule lumen. It marks stable microtubules and is required for polarity establishment and directional migration. Here we elucidate the mechanistic underpinnings for TAT activity and its preference for microtubules with slow turnover. 1.35 Å TAT cocrystal structures with bisubstrate analogs constrain TAT action to the microtubule lumen and reveal Lys40 engaged in a suboptimal active site. Assays with diverse tubulin polymers show that TAT is stimulated by microtubule inter-protofilament contacts. Unexpectedly, despite the confined intraluminal location of Lys40, TAT efficiently scans the microtubule bidirectionally and acetylates stochastically without preference for ends. First-principles modeling and single-molecule measurements demonstrate that TAT catalytic activity, not constrained luminal diffusion, is rate-limiting for acetylation. Thus, because of its preference for microtubules over free tubulin and its modest catalytic rate, TAT can function as a slow clock for microtubule lifetimes.

*Correspondence should be addressed to: Antonina Roll-Mecak, Cell Biology and Biophysics Unit, Porter Neuroscience Research Center, National Institutes of Health, Building 35, Room 3B-203, 35 Convent Drive, MSC 3700, Bethesda, MD 20892-3700, Telephone: 301-814-8119, Antonina@mail.nih.gov.

†these authors contributed equally and are listed in random order

‡Present address Department of Molecular Biology, Cell Biology and Biochemistry, Brown University, Providence, RI 02903, U.S.A.

Accession codes

Atomic coordinates and structure factor amplitudes have been deposited in the Protein Data Bank (PDB ID ### and ###)

AUTHOR CONTRIBUTIONS

A.R.-M. conceived the project and planned experiments together with all authors. A.S. solved structures together with A.R.-M., performed activity assays; A.M.D. performed EM and interpreted data together with N.G.; J.S. performed TIRF assays and diffusion calculations, B.G., immunofluorescence, M.L.V. TIRF assays with MAPs and yeast microtubules and N.E.Z. microtubule binding assays. A.R.-M. wrote the manuscript with help from A.M.D. and J.S. The manuscript was reviewed by all authors.

COMPETING FINANCIAL INTERESTS

The authors declare no competing financial interests.

Author Manuscript Author Manuscript Author Manuscript Author Manuscript

INTRODUCTION

Microtubules are biopolymers constructed by the dynamic association of αβ-tubulin heterodimers and are essential for fundamental cellular processes ranging from intracellular transport to cell division and cellular morphogenesis. Cells constantly adapt their microtubule arrays to physiological needs by modulating the balance between dynamic short-lived, and stable long-lived microtubule subpopulations. For example, during neurite extension, dynamic microtubules drive the growth of a new neurite, while stable microtubules provide the infrastructure to support this cell elongation (Tahirovic and Bradke, 2009). Microtubules are subject to diverse and evolutionarily conserved posttranslational modifications (Garnham and Roll-Mecak, 2012; Wloga and Gaertig, 2010). While the majority of these modifications are on the exterior of the microtubule, acetylation on α-tubulin Lys40 stands out as the only modification in the microtubule lumen and characterizes old, stable microtubules (Greer et al., 1985; L'Hernault and Rosenbaum, 1985; LeDizet and Piperno, 1987; Piperno and Fuller, 1985; Piperno et al., 1987; Schulze et al., 1987). Studies using antibodies specific for acetylated tubulin revealed that acetylation occurs primarily on microtubules and not tubulin, and that it is especially abundant on stable microtubules found in cilia, flagella and centrioles, as well as on subsets of microtubules in the mitotic spindle and long-lived cytoplasmic microtubules with slow dynamics ($t_{1/2}$ > 2hrs) that are resistant to depolymerization (Black et al., 1989; Piperno and Fuller, 1985; Piperno et al., 1987; Schulze et al., 1987; Webster and Borisy, 1989). Moreover, stabilization of cellular microtubules using taxol or microtubule associated proteins (MAPs) increases acetylation levels (Piperno et al., 1987; Takemura et al., 1992).

Tubulin posttranslational marks, including acetylation, are read by molecular motors and can be used to target them and their cargo to subpopulations of microtubules that have been selectively stabilized (Cai et al., 2009; Hammond et al., 2010). Consequently, tubulin acetylation is important for early polarization events in neurons (Hammond et al., 2010; Reed et al., 2006), and decreased tubulin acetylation is linked to defective axonal transport and neuronal migration as well as neurodegenerative disorders such as Alzheimer's, Huntington's and Charcot-Marie-Tooth diseases (Dompierre et al., 2007; Li et al., 2012; reviewed in Garnham and Roll-Mecak, 2012). Moreover, deficits in axonal transport can be rescued by tubulin hyperacetylation (Dompierre et al., 2007).

Tubulin acetyltransferase (TAT) is required for mechanosensation in *C. elegans* (Akella et al., 2010; Shida et al., 2010). Acetylation does not seem to be only a passive mark on the microtubule, as its loss disrupts microtubule structural integrity in touch receptor neurons, leading to axonal morphology defects (Cueva et al., 2012; Topalidou et al., 2012). TAT loss also causes neuromuscular defects in zebrafish (Akella et al., 2010) and brain abnormalities in mice (Kim et al., 2013). Studies in *C. elegans* show that TAT loss disrupts microtubule-based motor transport in axons, leading to spontaneous adult-onset axonal degeneration that worsens with age and axon length (Neumann and Hilliard, 2014).

Other than viruses and clathrin cages, microtubules are the only known hollow polymers in eukaryotic cells. Acetylation on Lys40 stands out as the only known tubulin posttranslational modification located in the microtubule lumen (Nogales et al., 1999;

Author Manuscript Author Manuscript Author Manuscript Author Manuscript

Soppina et al., 2012). To understand the mechanism of any enzyme, it is critical to know how it accesses its substrate. TAT presents a puzzle: its activity is stimulated by microtubules, yet the luminal presentation of Lys40 within microtubules hinders access by the enzyme. How TAT accesses Lys40 in the microtubule lumen is still not understood. It has been proposed that TAT accesses the lumen either by diffusing from ends (Akella et al., 2010) or taking advantage of defects or breathing of the microtubule lattice. The latter would either allow transient access of the enzyme to the lumen or enable excursion of the Lys40 loop to the exterior of the microtubule shaft (Howes et al., 2014; Shida et al., 2010; Yajima et al., 2012). To elucidate substrate access by TAT and to uncover the molecular basis for the *in vivo* correlation between acetylation and microtubule age, we combined X-ray crystallography, electron microscopy, biochemical and single-molecule fluorescence analyses, and modeling. We report the first crystal structure of TAT in complex with a tubulin peptide–ac-CoA bisubstrate analog that together with structure-based functional analyses constrains the active enzyme to the microtubule lumen. Unexpectedly, we find that acetylation by TAT proceeds stochastically along the microtubule without a preference for ends despite the luminal location of the acetylation site. Consistent with this, single-molecule fluorescence imaging reveals that TAT efficiently and stochastically scans the microtubule, while modeling and kinetic analyses demonstrate that TAT catalytic activity, rather than access to the luminal acetylation site, is rate-limiting. Thus, by virtue of its preference for the microtubule geometry and its low catalytic rate, TAT alone can function as an enzymatic timer for microtubule lifetimes.

RESULTS

Tubulin Lys40 loop recognition by TAT

Lys40 lies in a twenty-amino acid loop (Gigant et al., 2005; Nogales et al., 1999; Nogales et al., 1998). Although α-tubulin residues 37–42 are stringently conserved in α-tubulin isoforms with an acetylatable lysine, the ten-residue segment encompassing Lys40 is disordered in cryo-EM reconstructions of microtubules, indicating high flexibility. To visualize at atomic resolution the conformation of the Lys40 loop when engaged by TAT, and to characterize the Lys40 loop-binding surface of the enzyme, we determined the first structures of human TAT bound to its substrate lysine, by co-crystallizing it with two distinct bisubstrate analogs consisting of a substrate peptide covalently linked to CoA through Lys40 (Figures 1, S1 and Experimental Procedures). Such analogs have been extensively employed to analyze the catalytic mechanism of other lysine acetyltransferases (*e.g.* p300/CBP (Liu et al., 2008) and GCN5 (Poux et al., 2002)). In general, bisubstrate analogs have been important tools for understanding the mechanism of enzymes that link two substrates. Our two 1.35 Å resolution complex structures (Table S1) exhibit no significant differences between them (r.m.s.d = 0.1Å over all atoms). The high resolution of our structures (coordinate precision ∼ 0.1 Å) provides detailed insights into TAT recognition of the Lys40 loop.

The TAT core consists of a six-stranded β-sheet surrounded by five α-helices (Figure 1). The CoA is cradled between strand β6 and helix α5 (Friedmann et al., 2012; Kormendi et al., 2012; Taschner et al., 2012). Our structures now show residues 38–41 of the α-tubulin

Author Manuscript Author Manuscript Author Manuscript Author Manuscript

acetylation loop folding as an irregular turn (Figure 1B), packing against a funnel-shaped depression in the TAT surface (Figures 2A and B), and presenting a fully extended Lys40 into the active site (Figure 1C). The external margin of the TAT funnel is formed by residues from the α2-α3 loop, α3, the loop preceding β8, and the β7-α5 loop (Figure 1A) that make direct and water-mediated hydrogen bonds with the substrate peptide (Figure 1B).

Asp157 of TAT plays a key role at the enzyme-tubulin interface, coordinating the tubulin peptide backbone *via* a bi-dentate hydrogen bond to the backbone amides of α-tubulin Asp39 and Lys40 (Figure 1B). Consistent with this, mutation of TAT Asp157 reduces acetylation by ∼96% and 92% with tubulin and microtubules, respectively (Figure 2C). The Lys40 backbone is further stabilized by a water-mediated hydrogen bond between its main-chain carbonyl and the side chain of conserved Asn182 of TAT (Figure 1B). Mutation of TAT residues Arg69, His75 and Lys98, which stabilize α-tubulin Asp39, significantly impairs activity (Taschner et al., 2012) (Figure 2C). Likewise, mutation of invariant Asn182 of TAT, which hydrogen-bonds with α-tubulin Ser38, is detrimental (Figures 1B and 2C). The many water-mediated interactions between the α-tubulin peptide and TAT suggest a labile interface, consistent with TAT's modest affinity for and activity with the tubulin peptide (Figure S1B). The peptide N-terminus is cradled by invariant Phe183 and Leu104 of TAT, while the carbonyl oxygen preceding α-tubulin Ser38 hydrogen bonds with invariant Lys102. Mutation of Lys102 renders TAT inactive with α-tubulin peptide (data not shown) and reduces its activity ∼87% with tubulin and microtubules (Figure 2C). The extended Lys40 projects into the funnel neck lined by conserved TAT residues (Figures 1C and 2A). Direct and water-mediated hydrogen bonds between invariant Gln58 and Arg158 of TAT close the front of the funnel. The Lys40 side chain is stabilized by van der Waals contacts with conserved Ile64 and the aliphatic moieties of invariant Arg158 and Asp157. Consistent with their role in Lys40 coordination, mutation of Arg158 and Ile64 reduce TAT activity by ∼ 70 % and >90%, respectively (Taschner et al., 2012).

Active site architecture

To be acetylated, the ε-ammonium group of Lys40 needs to be deprotonated. This is followed by nucleophilic attack by the amine on the carbonyl carbon of ac-CoA. The invariant Asp157 of TAT is well positioned to deprotonate the Lys40 ε-ammonium as it enters the hydrophobic substrate tunnel. Thus, Asp157 may play a role not only in substrate binding, but also catalysis, consistent with the severely deleterious effects of its mutation (Figure 2C). Further catalysis could be achieved by enhancing nucleophilicity of the amine by a general base. Cys120 was proposed to act as a catalytic residue (Friedmann et al., 2012). Our structure shows that Cys120 approaches no closer than 10.6 Å the amide of the bisubstrate analog (Figure 1B), making it an unlikely catalytic residue. Gln58, also proposed to be a catalytic residue (Taschner et al., 2012) is well positioned to hydrogen bond to the transition state (its side-chain amide oxygen lies 2.9 Å from the carbonyl oxygen of the bisubstrate analog linker). It is, however, unlikely to function in deprotonating the incoming α-tubulin Lys40, since its mutation to glutamate, a better base, abolishes TAT activity (Figure 2C). Moreover, while conserved across vertebrate TATs, Gln58 is replaced by Leu in nematode TAT. Gln58 is stabilized by Asp123 whose mutation also decreases TAT activity to background levels (Figure 2C). Asp123 is unlikely to deprotonate Lys40, since it

Author Manuscript Author Manuscript Author Manuscript Author Manuscript

approaches no closer than 5.5 Å from the Lys40 nitrogen atom and is more likely important in orienting the Gln58 side chain. Overall, consistent with the low catalytic rate exhibited with tubulin (0.4 h^{-1}), our structure shows that the active site of TAT is not optimized for efficient proton transfer.

The TAT-tubulin intermolecular interface

The Lys40 portal bisects a belt of conserved residues on the TAT surface (Figures 2B and S2) that extends beyond the Lys40 loop recognition funnel and likely constitutes an interaction surface with the rest of tubulin and the microtubule. This surface is flanked by helix α2 and the β4-β5 hairpin, a structural element unique to the TAT family and not found in the related GCN5 family acetyltransferases (Friedmann et al., 2012; Kormendi et al., 2012; Taschner et al., 2012). Mutation of conserved Phe189 and Phe190 that support the β4-β5 hairpin reduces TAT activity to background (Figure 2C). Mutation of invariant Phe105 protruding from the β4-β5 hairpin (Figure 2B) severely impairs enzyme activity with both tubulin and microtubules while still preserving 89% activity with a 15-residue tubulin peptide (data not shown), implicating this residue in tubulin recognition beyond the Lys40 loop. Interestingly, mutation of conserved residues in helix α2 (I47A, D48A and K52A, S54A) impairs acetylation disproportionately with microtubules over tubulin, indicating that this structural element is important for sensing the microtubule. α2 contains one of the most conserved TAT sequence segments, underscoring its functional importance.

Lateral lattice interactions dominate microtubule enhancement of TAT activity

TAT activity is enhanced with microtubules over tubulin (Akella et al., 2010; Kormendi et al., 2012; Maruta et al., 1986; Shida et al., 2010). Microtubules grow through the longitudinal head-to-tail association of tubulin dimers into protofilaments and through lateral interactions, protofilaments associate side-by-side into the cylindrical microtubule. As a step towards localizing the site of TAT action, we sought to identify the microtubule lattice contacts critical for this enhancement. The Lys40 loop lies at the vertex of four tubulin heterodimers in the microtubule (Nogales et al., 1999). Thus, TAT activity can be impacted by both longitudinal (between tubulin heterodimers in a protofilament) and lateral (between neighboring protofilaments) lattice contacts (Figure 3). To understand the relative contribution of longitudinal *versus* lateral contacts for TAT function we compared TAT activity on microtubules and on tubulin polymers with distinctly different geometries generated using either peptides or certain cations. All these polymers involve longitudinal interactions between tubulin dimers, and a varying inter-dimer angle and polymer curvature (Figure 3A). Stathmin/Op18 strings two tubulin dimers head to tail (α1β1-α2β2) in a slightly curved configuration (Gigant et al., 2005). Dolastatin-10, a short peptide, induces tubulin rings by curving individual protofilaments such that their luminal surface becomes exposed on the exterior face of the ring (Mulder et al., 2009). Zn^{2+} induces the formation of tubulin sheets in which protofilaments of alternating polarity are arrayed in parallel (Nogales et al., 1998). Acetylation assays with these substrates revealed a statistically significant enhancement over unpolymerized tubulin, indicating a minor contribution of longitudinal lattice contacts to TAT stimulation by microtubules, as well as a lack of strong curvature dependence (Figure 3A).

Author Manuscript Author Manuscript Author Manuscript Author Manuscript

The largest activity enhancement over unpolymerized tubulin is seen with microtubules, which unlike the other polymers tested, display lateral interactions in addition to longitudinal ones. TAT's preference for microtubules manifests itself in both enhanced catalytic rate and higher affinity (Figure 3A and S3). While stable complex formation between unpolymerized tubulin and TAT was undetectable by analytical ultracentrifugation at TAT concentrations as high as 40 μM, binding of TAT to microtubules was evident in sedimentation assays, albeit with a modest affinity ($K_d \sim 44$ μM; Figure S3B and C), comparable to the reported K_m for the enzyme (~ 32 μM; (Friedmann et al., 2012)). Consistent with the importance of lateral interactions for TAT binding, we find that the enzyme promotes stacking of dolastatin-induced tubulin rings in a dose-dependent manner (Figures S3D) as previously found for kinesin-13, which is thought to interact with adjacent protofilaments while promoting microtubule depolymerization (Mulder et al., 2009). The F105A TAT mutant defective in acetylation is also impaired in stack formation (Figure S3E). The relatively high TAT concentration needed for stack formation is consistent with the modest affinity of TAT for the microtubule. Interestingly, in *C. elegans* mechanosensory neurons, TAT is one of the most highly expressed genes, at levels comparable to tubulin (Topalidou et al., 2012; Zhang et al., 2002).

Steric constraints on Lys40 recognition

Our structures reveal the conformation of the Lys40 loop when engaged by TAT and thus provide constraints on its presentation to the enzyme in the microtubule context. Residues 38–47 of α-tubulin are invisible in current EM reconstructions of microtubules (Fourniol et al., 2010; Maurer et al., 2012), but reliable density is present for Pro37. Pro37 is more than 25 Å from the outside microtubule surface, and just two residues away from Lys40 (a maximum span of 12 Å were the polypeptide fully stretched), implying that Lys40 cannot reach out of the lumen without significant rearrangements in microtubule structure (Figure 3B). Deuterium exchange experiments revealed no differences in regions flanking the Lys40 loop in tubulin *versus* microtubules (Xiao et al., 2006), underscoring the stability of these secondary structure elements. The Lys40 loop lies beneath a fenestration at the vertex formed by four tubulin dimers (Figure 3B). It has been proposed that this fenestration could allow access of TAT to Lys40 from the outside of the microtubule (Yajima et al., 2012). However, accessing Lys40 from the outside would still require a long, convex protuberance. Importantly, the TAT microtubule recognition surface, defined by our structures and functional analyses is concave, thus not satisfying shape complementarity principles. Thus, our structural and functional data suggest that large rearrangements of the microtubule or TAT would be needed in order for TAT to reach Lys40 from the microtubule exterior. We cannot completely rule out transient, large openings in the lattice that could expose enough of the luminal space to allow TAT to bind Lys40 without completely entering the lumen as previously proposed (Shida et al., 2010). However, our experiments with tubulin polymers of different geometries show that lateral lattice interactions are key to TAT activity. These interactions would not be present at microtubule lattice openings.

TAT acetylation is stochastic along the microtubule

Based on the luminal location of the acetylation site, it was proposed that TAT activity on microtubules would be impaired due to hindered access to Lys40 (Akella et al., 2010; Odde,

Author Manuscript Author Manuscript Author Manuscript Author Manuscript

1998; Shida et al., 2010). This model is consistent with studies showing that acetylation of axonemes proceeds as a gradient from microtubule ends (Akella et al., 2010), suggestive of a diffusive mechanism along their axis. Interestingly, acetylation on microtubules in cells does not show a gradient from microtubule ends and appears randomly distributed. To elucidate TAT's direct contribution to these observed acetylation patterns, we visualized the distribution of acetylation marks introduced by recombinant TAT *in vitro* on microtubules using an antibody specific for acetylated tubulin. We find that TAT acetylates along the entire microtubule without a preference for ends (Figure 4). The slow accumulation of acetylation marks on microtubules (over tens of minutes) is consistent with the low acetylation rate observed in bulk measurements ($\sim$1.6 h^{-1}) as well as cells (Piperno et al., 1987). The longitudinally unbiased, punctate acetylation pattern is similar to that observed on microtubules in cells (Piperno et al., 1987; Webster and Borisy, 1989). We also observe a stochastic distribution of acetylation on non-taxol stabilized microtubules indicating that this effect cannot be attributed to taxol (Figure S4). Furthermore, we examined the acetylation distribution under conditions where TAT is not limiting. Early time points show again that the enzyme accesses different sites along the entire microtubule equally well and without a bias for sites close to the ends or restricted regions that could signal lattice defects (Figure 4C). This is apparent in the line-scan of a microtubule at an early time point, and also in average line-scans of multiple microtubules, which demonstrate a uniform acetylation probability along the microtubule (Figure 4D).

TAT scans the microtubule lumen using surface diffusion

To understand the mechanism underlying the unbiased acetylation distribution on microtubules and to understand how TAT is able to access the luminal acetylation site, we examined the dynamics of TAT on microtubules. We employed single-molecule total internal reflection fluorescence (TIRF) microscopy to visualize purified TAT-GFP on microtubules immobilized on coverslips (TAT-GFP activity is comparable to that of the untagged protein, Figure S5). We observe that single TAT-GFP molecules scan microtubules bidirectionally with a mean 1D diffusion coefficient of 0.27 $\mu m^2/s$ (Figures 5A and 5B). The average interaction time (τ) of TAT-GFP on microtubules is 1.5 s (Figure 5C) and the average microtubule length scanned by a TAT molecule is 2.9 μm, with excursions up to 10.4 μm (Figure S5B). The positions where TAT-GFP molecules start their scans are randomly distributed on the microtubule, showing no bias for ends (Figure 5D and S5C). Two possible explanations for this observation are, (1) TAT scans the outside of the microtubule in order to more efficiently find ends or lattice defects that allow it access to the Lys40 loop. TAT access through transient lattice openings has been previously proposed (Howes et al., 2014; Shida et al., 2010); (2) TAT enters the microtubule lumen through the ends and diffuses through the lumen where it is randomly retarded by its affinity for the microtubule wall. TAT diffusion is too fast to observe when not retarded by the interaction with the microtubule (see below and Experimental Procedures); therefore, the random distribution of scanning start sites would reflect the stochastic distribution of binding events.

Scanning on the microtubule exterior has been observed for the depolymerizing kinesin MCAK (Helenius et al., 2006) and tau (Hinrichs et al., 2012). MCAK uses this mechanism to find microtubule ends more efficiently (Helenius et al., 2006). One-dimensional diffusion

Author Manuscript Author Manuscript Author Manuscript Author Manuscript

is also used by DNA binding proteins to scan long DNAs for specific sequences (von Hippel and Berg, 1989). TAT robustly scans subtilisin-treated microtubules lacking the tubulin C-terminal tails (Figure 5E), unlike MCAK and tau that use these negatively charged tails for this process (Helenius et al., 2006; Hinrichs et al., 2012). Analysis of 50 microtubules shows that TAT scanning covers the same total microtubule length, regardless of whether microtubules are subtilisin-treated or untreated (Figure 5F, upper panel). A recent study reported a weak effect of the C-terminal tails on TAT microtubule binding (Howes et al., 2014). Here we find that microtubule acetylation is unaffected by removal of the C-terminal tails (Figure 5F, lower panel). Tubulin C-terminal tails are subject to abundant posttranslational modifications and acetylated microtubules in the cell are often also polyglutamylated, leading to the hypothesis that acetylation can be affected by these other modifications (Howes et al., 2014). However, we find that TAT scans unmodified microtubules and acetylates them as effectively as brain microtubules that are heavily polyglutamylated on C-terminal tails (Figures S5G and S5H). *Sacharomyces cerevisiae* α-tubulin does not have a conserved acetylation loop and TAT is absent in this organism. We do not observe TAT-GFP scanning on purified *S. cerevisiae* microtubules nor on engineered *S. cerevisiae* microtubules in which the divergent endogenous C-terminal tails were replaced with human C-terminal tails (Extended Experimental Procedures).

To establish whether scanning occurs on the outer surface of the microtubule or intra-luminally, we decorated the external microtubule surface with three microtubule binding proteins with distinct binding modes (doublecortin, spastin and the motor domain of kinesin-5), and measured both TAT scanning and acetylation activity (Figures 5 and S5). Doublecortin covers the fenestration at the vertices between four tubulin dimers that overlie the Lys40 loop (Fourniol et al., 2010) and that was proposed to allow access of TAT to the microtubule lumen from the outside. Addition of saturating concentrations of doublecortin had no effect on TAT-GFP microtubule scanning (τ = 1.4 s compared to 1.5 s for undecorated microtubules) or acetylation rates (Figures 5E, 5F and S5K). Interestingly, TAT localizes to doublecortin decorated microtubules *in vivo* (Kim et al., 2013). Saturating concentrations of spastin or kinesin likewise had no effect (Figures 5F and S5I). Under our experimental conditions, the microtubules were saturated with these MAPs (Figure S5J). We also used Dylight 550 labeled spastin to visualize microtubule decoration (Figure 5G). Microtubules coated with labeled spastin were also scanned efficiently by TAT (τ = 1.5 s, statistically indistinguishable from that on undecorated microtubules). Maximum intensity projections demonstrate that total microtubule coverage by TAT-GFP was unchanged in the presence of doublecortin, kinesin or spastin (Figure 5F, upper panel). Together, the results of our experiments with microtubules missing the C-terminal tails as well as decorated with various MAPs argue that TAT-GFP scans the microtubule lumen.

Recent cryo-electron reconstructions revealed Fab fragments (MW ∼50 kDa) of IgG 6–11B-1 antibodies against acetylated Lys40 arranged in regular arrays inside the microtubule lumen (Soppina et al., 2012). Surprisingly we find that even larger, full-length IgG 6–11B-1 antibodies can gain access to the lumen of taxol-stabilized acetylated microtubules. Negative-stain EM of microtubules incubated with these antibodies revealed two distinct populations (Figures S6A–E): one had an evident protofilament structure and displayed a 4

Author Manuscript Author Manuscript Author Manuscript Author Manuscript

nm layerline, reflecting the spacing underlying the helical structure of the microtubule because of the α/β tubulin equivalency at low resolution; the second showed a hardly discernible protofilament structure in real space and an additional 8 nm layerline in Fourier space (Figure S6E) indicative of the antibody binding to the tubulin heterodimer. Decorated microtubules showed no additional density along the edges, indicating that binding occurs on the luminal surface. In contrast, a well-characterized antibody that binds to the outer surface (directed against the α-tubulin C-terminal tail) showed clear density along microtubule edges (Figure S6F). Moreover, 6–11B-1 IgG also clustered at sites of microtubule mechanical damage where the lumen is exposed (Figure S6G). Taken together, these data indicate that an intact IgG antibody with affinity for the Lys40 loop can enter the microtubule.

Since our EM studies show that a particle as large as an antibody (relative dimensions of IgG and our TAT construct shown in Figure S6H) can gain access to the microtubule lumen (inner diameter 15 nm) on a time scale of tens of minutes (comparable to acetylation rates), we coupled a C-terminally biotinylated TAT construct to streptavidin beads 1 μm in diameter (experiments using 200 nm beads yielded the same results; data not shown). We then compared the activity of the bead-coupled TAT with tubulin and microtubules. While the bead-coupled enzyme retained activity with tubulin, activity with microtubules was reduced ∼89% (Figure 6A). The residual activity is likely due to unpolymerized tubulin (∼15%) present in these experiments. Overall, our experiments with engineered and bead-coupled TAT are consistent with a requirement for the enzyme to enter a confined space during acetylation and our experiments with MAP coated microtubules indicate that TAT is able to scan the luminal microtubule wall using surface diffusion.

We cannot completely rule out that there are defects in the lattice that would allow the enzyme to enter at “breathing” points along the microtubule as proposed (Friedmann et al., 2012; Howes et al., 2014; Shida et al., 2010; Soppina et al., 2012). This could account for the random distribution of acetylation marks as well as TAT trajectories that we observe. Defects on the order of 1–2 nm have been documented in microtubules *in vitro* at points where there are protofilament number changes (Chretien et al., 1992); however these defects are sparse, the spacing between them ranging from 2.6 μm to more than 20 μm (Chretien et al., 1992), not consistent with the non-biased acetylation patterns that we see on microtubules. The diameter of the TAT globular core is ∼ 5 nm, imposing a lower bound on the size of these possible defects on the order of at least one tubulin dimer. Notably, microtubule acetylation is especially abundant on cilia and neuronal microtubules that are covered with stabilizing MAPs. In our assays acetylation or TAT scanning are not impaired on microtubules coated with doublecortin that binds at the vertex of four tubulin dimers and stabilizes longitudinal and lateral lattice interactions. Moreover, TAT mobility (Figure 5) and acetylation patterns (Figure 4) on the microtubule do not show a bias towards specific regions that would suggest lattice defects (Figure S5C).

TAT catalytic rate, not Lys40 accessibility, is rate limiting

The stochastic distribution of acetylation marks and TAT scanning trajectories argues against access to Lys40 being limiting for microtubule acetylation. We applied a previously

Author Manuscript Author Manuscript Author Manuscript Author Manuscript

derived first-principles model to TAT diffusion that accounts for microtubule wall hindrance effects and reversible binding to describe diffusion through the 15 nm wide microtubule lumen of particles with varying size and microtubule affinity (Bungay and Brenner, 1973; Odde, 1998). Our calculations (Experimental Procedures) indicate that the TAT (Stokes radius R_H=2.7 nm) equilibration time between the microtubule outside and inside would be on the order of minutes for a 10 μm-long microtubule (open on both ends), the mean length of microtubules in our experiment (Figure 6B and Figure S4E). This is consistent with our observation that, when in excess, TAT acetylates unhindered along the entire microtubule on the order of minutes (Figure 4C). The equilibration time depends primarily on TAT dimensions and affinity for the microtubule wall and is very sensitive to the latter parameter (Odde, 1998) (Experimental Procedures and Figure S6I). Our calculations show that TAT diffusion is retarded three orders of magnitude by luminal confinement and microtubule binding. At our current frame acquisition rates, we are unable to detect TAT-GFP diffusion through the microtubule when TAT is not retarded (calculated D_{hindered}=26.3 $\mu m^2/s$, Experimental Procedures). Thus, the random distribution of scanning trajectory starting points (Figure 5D) most likely reflects the stochastic nature of the TAT-microtubule interaction, *i.e*. TAT can be observed in our assays only when retarded by its interaction with the microtubule.

DISCUSSION

Stable microtubules in cells, but not dynamic microtubules, are marked by acetylation at Lys40. In the absence of acetylation by TAT, microtubule structural integrity is affected and cell polarity is perturbed in cells that are particularly dependent on stable, polarized microtubule arrays, such as neurons (Cueva et al., 2012; Li et al., 2012; Neumann and Hilliard, 2014; Topalidou et al., 2012). But, how are stable microtubules selectively marked for the action of regulators? Our results indicate that microtubule age-dependent acetylation by TAT is achieved not by impaired diffusion because of the luminal location of the acetylation site, but due to the slow enzymatic rate of TAT that is more than an order of magnitude slower than the lifetime of dynamic microtubules ($t_{1/2} \sim$ 5min) and more closely matched to the lifetime of stable microtubules ($t_{1/2} >$ 2 hrs) in cells (Schulze et al., 1987; Schulze and Kirschner, 1987; Webster and Borisy, 1989). Acetylation is especially enriched on microtubule populations with extremely slow dynamics ($t_{1/2} \sim$ 16 hrs; (Webster and Borisy, 1989)) that are a hallmark of postmitotic cells with complex microtubule architectures such as neurons (Black et al., 1989). The cell solves the problem of selective marking a stable microtubule population by having a modification inside the microtubule lumen, and then exploiting the kinetic discordance between the rate of one-dimensional diffusion *versus* the catalytic constant of the tubulin acetylase. Acetylation is reversed in cells by the action of tubulin deacetylases such as HDAC6 and SIRT2 (Hubbert et al., 2002; North et al., 2003). The accumulation of acetylated stable microtubules in cells implies that the reverse deacetylation reaction is even slower than TAT microtubule acetylation. TAT activity defines the population of microtubules that would be available for deacetylases to act on, i.e. stable microtubules because dynamic microtubules would not persist long enough for TAT to acetylate them. However, the density of the acetylation mark on stable microtubules does depend on the activity of deacetylases. I*n vivo*, deacetylation is strongly

Author Manuscript Author Manuscript Author Manuscript Author Manuscript

coupled with microtubule depolymerization (Black et al., 1989), thus resetting the age dependent acetylation clock. The net acetylation level and the steepness of the acetylation gradient from old to new will be modulated by overall deacetylase activity. Thus, TAT can function as an enzymatic timer for microtubules with slow turnover and mark them selectively for the action of microtubule regulators.

Our kinetic analyses and modeling show that TAT diffusion is markedly faster than its catalytic rate, explaining the lack of an acetylation gradient on microtubules as would be expected for a diffusion-limited reaction. Consistent with access to the luminal modification site not being limiting, acetylation rates are not enhanced when TAT is copolymerized with tubulin (Kalebic et al., 2013) and acetylation *in vivo* lags tens of minutes behind microtubule polymerization (Black et al., 1989; Piperno et al., 1987). Earlier experiments show that acetylation is not enhanced when microtubules are shortened by shearing (Maruta et al., 1986). In order to produce an observable gradient, microtubules would have to be sufficiently long to match the catalytic rate of TAT. Such an effect would become observable at microtubule lengths exceeding 75 μm (or 150 μm if both ends are open; Figure S6J). Microtubule lengths *in vivo* range between 1–100 μm (Odde, 1998). In the shearing experiments the mean lengths were reduced from ∼ 3.4 to 0.6 μm, a length regime where no diffusion limiting effects would have been seen fifteen minutes into the reaction when acetylation was measured (Maruta et al., 1986). Thus, our experiments (Figures 4 and 5) as well as kinetic modeling (Figure 6B) indicate that substrate access through microtubule ends would not be rate limiting for acetylation by TAT, but catalytic rate is. While microtubule defects could further facilitate TAT access to the luminal microtubule space *in vivo*, they are not required for TAT access on timescales of the order of the catalytic rate of the enzyme. Unlike kinesins that have been shown to act as microtubule rulers by selectively tagging and enhancing their activity on longer microtubules (Subramanian et al., 2013; Varga et al., 2009), TAT can act as a timer for microtubule lifetimes and can effectively mark stable microtubules, both long and short.

Consistent with the slow catalytic rate of the enzyme, our crystal structures of TAT with two bisubstrate analogs reveal an active site not optimized for efficient catalysis (Figures 1, 2, and S1E). To accumulate a Michaelis complex and achieve reactivity in this regime of low k_{cat}, the off-rate of the enzyme would have to be slow. However, in such a situation, the enzyme would have limited coverage of the microtubule length in conditions where TAT is limiting because it would be retained close to the microtubule end. We speculate that scanning of the microtubule *via* surface diffusion allows TAT to remain associated with the microtubule in a reactive state for longer periods and yet achieve coverage of long microtubule spans. The high degree of hydration at the TAT-Lys40 loop interface revealed by our cocrystal structures could facilitate the diffusion along the microtubule, akin to the “water lubricated” 1D diffusion proposed to be important for the diffusion of DNA binding proteins along DNA (Cooper and Wordeman, 2009).

Electron cryo-tomography revealed discrete, closely spaced particles decorating the lumen of flagellar (Nicastro et al., 2006; Sui and Downing, 2006) and neuronal (Garvalov et al., 2006; Topalidou et al., 2012) microtubules. Future experiments will clarify how TAT access is modulated by the presence of luminal particles. Interestingly, these particles disappear

Author Manuscript Author Manuscript Author Manuscript Author Manuscript

from the lumen of neuronal microtubules upon rapid disassembly and reassembly (Burton, 1984), suggesting a microtubule-age dependent accumulation process. In addition to providing a molecular basis for age dependent microtubule acetylation, our studies are also applicable to the microtubule binding behavior of other proteins with luminal localization found in neuronal microtubules and axonemes. Furthermore, the interplay between TAT acetylation activity in the constrained luminal space and the association of the enzyme with larger complexes in the cell will be an interesting area of future exploration.

EXPERIMENTAL PROCEDURES

Protein production, crystallization and X-ray structure determination

Homo sapiens TAT (1–196) was expressed in *Eschericia coli* as a GST-fusion and purified by standard chromatography techniques. A reversed-phase HPLC assay shows that TAT acetylates minimal tubulin-derived peptides, albeit at a rate ∼40-fold lower than with tubulin (Figures S1A and S1B), demonstrating that the minimal requirements for catalysis are satisfied by the engagement of TAT with an α-tubulin-derived peptide. The existence of a ternary complex between TAT, ac-CoA and its tubulin substrate is supported by previous kinetic analyses (Friedmann et al., 2012), justifying the use of bisubstrate analogs as functional mimics of a TAT ternary complex. Two bisubstrate analogs (Figures S1C and S1D) yielded co-crystals that diffracted to better than 1.35 Å resolution. Details for crystallization, structure determination and purification of TAT constructs can be found in Extended Experimental Procedures.

Acetylation Assays

Tubulin and microtubule acetylation assays with various mutants were performed using ^{3}[H]acetyl-coA as in (Kormendi et al., 2012). Acetylation assays with peptides, various tubulin polymers, in the presence of MAPs as well as bead-coupled TAT are described in Extended Experimental Procedures.

Modeling TAT diffusion

To assess the diffusion rate of TAT inside the microtubule, we used a previously developed mathematical model (Bungay and Brenner, 1973; Odde, 1998) that approximates the diffusing molecule as a sphere in a cylindrical pore and accounts for translational diffusion, hindrance due to the microtubule wall and the reversible binding of the molecule to the microtubule at dilute concentrations below K_d. Details of the calculations can be found in Extended Experimental Procedures. The free diffusion coefficient of TAT is 79.3 $\mu m^2/s$. This indicates that a single TAT molecule travels an r.m.s. distance of 3.9 μm in ∼ 0.1 seconds. TAT diffusion inside a microtubule is further hindered by the microtubule wall, resulting in a $D_{hindered}$ of 26.3 $\mu m^2/s$ (2.3 μm traveled in 0.1 seconds), given by the Bungay-Brenner relationship (Bungay and Brenner, 1973). TAT diffusion is most significantly retarded by its reversible binding to the microtubule lumen (Odde, 1998). This results in an effective diffusion constant of TAT $D_{effective} \sim 0.082\ \mu m^2/s$.

Author Manuscript Author Manuscript Author Manuscript Author Manuscript

TIRF imaging and analysis

Chambers for single molecule assays were assembled as described in (Ziolkowska and Roll-Mecak, 2013). GFP-TAT molecules were tracked using MTrackJ (Meijering et al., 2012). A complete description of data collection and analyses can be found in Extended Experimental Procedures.

Supplementary Material

Refer to Web version on PubMed Central for supplementary material.

Acknowledgments

We thank G. Piszczek (National Heart, Lung and Blood Institute Biophysics core) for AUC help, B. Castle and D. Odde (University of Minnesota) for modifying the TipTracker program, G. Brouhard (McGill University) for the doublecortin expression plasmid. A. R.-M. thanks A. Szabo for discussions on diffusion, A. Ferré-D'Amaré, E. Giniger, S. Gottesman, K. Swartz and R. Vale for critical reading of the manuscript. We are grateful to Chen Xu for training at the Brandeis University EM facility where the EM data was collected (supported by National Institutes of Health Grant P01 GM62580 awarded to N.G.). A.R.-M. is a Searle Scholar and supported by the intramural program of the National Institutes of Health.

References

Akella JS, Wloga D, Kim J, Starostina NG, Lyons-Abbott S, Morrissette NS, Dougan ST, Kipreos ET, Gaertig J. MEC-17 is an alpha-tubulin acetyltransferase. Nature. 2010; 467:218–222. [PubMed: 20829795]

Bechstedt S, Brouhard GJ. Doublecortin recognizes the 13-protofilament microtubule cooperatively and tracks microtubule ends. Dev Cell. 2012; 23:181–192. [PubMed: 22727374]

Black MM, Baas PW, Humphries S. Dynamics of alpha-tubulin deacetylation in intact neurons. J Neurosci. 1989; 9:358–368. [PubMed: 2563279]

Bungay PM, Brenner H. The motion of a closely-fitting sphere in a fluid-filled tube. Internaltional Jounral of Multiphase Flow. 1973; 1:25–56.

Burton PR. Luminal material in microtubules of frog olfactory axons: structure and distribution. J Cell Biol. 1984; 99:520–528. [PubMed: 6430914]

Cai D, McEwen DP, Martens JR, Meyhofer E, Verhey KJ. Single molecule imaging reveals differences in microtubule track selection between Kinesin motors. PLoS Biol. 2009; 7:e1000216. [PubMed: 19823565]

Chretien D, Metoz F, Verde F, Karsenti E, Wade RH. Lattice defects in microtubules: protofilament numbers vary within individual microtubules. J Cell Biol. 1992; 117:1031–1040. [PubMed: 1577866]

Cooper JR, Wordeman L. The diffusive interaction of microtubule binding proteins. Curr Opin Cell Biol. 2009; 21:68–73. [PubMed: 19185482]

Cueva JG, Hsin J, Huang KC, Goodman MB. Posttranslational acetylation of alpha-tubulin constrains protofilament number in native microtubules. Curr Biol. 2012; 22:1066–1074. [PubMed: 22658592]

Dompierre JP, Godin JD, Charrin BC, Cordelieres FP, King SJ, Humbert S, Saudou F. Histone deacetylase 6 inhibition compensates for the transport deficit in Huntington's disease by increasing tubulin acetylation. J Neurosci. 2007; 27:3571–3583. [PubMed: 17392473]

Fourniol FJ, Sindelar CV, Amigues B, Clare DK, Thomas G, Perderiset M, Francis F, Houdusse A, Moores CA. Template-free 13-protofilament microtubule-MAP assembly visualized at 8 A resolution. J Cell Biol. 2010; 191:463–470. [PubMed: 20974813]

Friedmann DR, Aguilar A, Fan J, Nachury MV, Marmorstein R. Structure of the alpha-tubulin acetyltransferase, alphaTAT1, and implications for tubulin-specific acetylation. Proc Natl Acad Sci U S A. 2012; 109:19655–19660. [PubMed: 23071314]

Author Manuscript Author Manuscript Author Manuscript Author Manuscript

Garnham CP, Roll-Mecak A. The chemical complexity of cellular microtubules: tubulin post-translational modification enzymes and their roles in tuning microtubule functions. Cytoskeleton. 2012; 69:442–463. [PubMed: 22422711]

Garvalov BK, Zuber B, Bouchet-Marquis C, Kudryashev M, Gruska M, Beck M, Leis A, Frischknecht F, Bradke F, Baumeister W, et al. Luminal particles within cellular microtubules. J Cell Biol. 2006; 174:759–765. [PubMed: 16954350]

Gigant B, Wang C, Ravelli RB, Roussi F, Steinmetz MO, Curmi PA, Sobel A, Knossow M. Structural basis for the regulation of tubulin by vinblastine. Nature. 2005; 435:519–522. [PubMed: 15917812]

Greer K, Maruta H, L'Hernault SW, Rosenbaum JL. Alpha-tubulin acetylase activity in isolated Chlamydomonas flagella. J Cell Biol. 1985; 101:2081–2084. [PubMed: 4066751]

Hammond JW, Huang CF, Kaech S, Jacobson C, Banker G, Verhey KJ. Posttranslational modifications of tubulin and the polarized transport of kinesin-1 in neurons. Mol Biol Cell. 2010; 21:572–583. [PubMed: 20032309]

Helenius J, Brouhard G, Kalaidzidis Y, Diez S, Howard J. The depolymerizing kinesin MCAK uses lattice diffusion to rapidly target microtubule ends. Nature. 2006; 441:115–119. [PubMed: 16672973]

Hinrichs MH, Jalal A, Brenner B, Mandelkow E, Kumar S, Scholz T. Tau protein diffuses along the microtubule lattice. J Biol Chem. 2012; 287:38559–38568. [PubMed: 23019339]

Howes SC, Alushin GM, Shida T, Nachury MV, Nogales E. Effects of tubulin acetylation and tubulin acetyltransferase binding on microtubule structure. Mol Biol Cell. 2014; 25:257–266. [PubMed: 24227885]

Hubbert C, Guardiola A, Shao R, Kawaguchi Y, Ito A, Nixon A, Yoshida M, Wang XF, Yao TP. HDAC6 is a microtubule-associated deacetylase. Nature. 2002; 417:455–458. [PubMed: 12024216]

Kalebic N, Martinez C, Perlas E, Hublitz P, Bilbao-Cortes D, Fiedorczuk K, Andolfo A, Heppenstall PA. Tubulin acetyltransferase alphaTAT1 destabilizes microtubules independently of its acetylation activity. Mol Cell Biol. 2013; 33:1114–1123. [PubMed: 23275437]

Kim GW, Li L, Gorbani M, You L, Yang XJ. Mice Lacking alpha-Tubulin Acetyltransferase 1 Are Viable but Display alpha-Tubulin Acetylation Deficiency and Dentate Gyrus Distortion. J Biol Chem. 2013; 288:20334–20350. [PubMed: 23720746]

Kormendi V, Szyk A, Piszczek G, Roll-Mecak A. Crystal structures of tubulin acetyltransferase reveal a conserved catalytic core and the plasticity of the essential N terminus. J Biol Chem. 2012; 287:41569–41575. [PubMed: 23105108]

L'Hernault SW, Rosenbaum JL. Chlamydomonas alpha-tubulin is posttranslationally modified by acetylation on the epsilon-amino group of a lysine. Biochemistry. 1985; 24:473–478. [PubMed: 3919761]

LeDizet M, Piperno G. Identification of an acetylation site of Chlamydomonas alpha-tubulin. Proc Natl Acad Sci U S A. 1987; 84:5720–5724. [PubMed: 2441392]

Li L, Wei D, Wang Q, Pan J, Liu R, Zhang X, Bao L. MEC-17 deficiency leads to reduced alpha-tubulin acetylation and impaired migration of cortical neurons. J Neurosci. 2012; 32:12673–12683. [PubMed: 22972992]

Liu X, Wang L, Zhao K, Thompson PR, Hwang Y, Marmorstein R, Cole PA. The structural basis of protein acetylation by the p300/CBP transcriptional coactivator. Nature. 2008; 451:846–850. [PubMed: 18273021]

Maruta H, Greer K, Rosenbaum JL. The acetylation of alpha-tubulin and its relationship to the assembly and disassembly of microtubules. J Cell Biol. 1986; 103:571–579. [PubMed: 3733880]

Maurer SP, Fourniol FJ, Bohner G, Moores CA, Surrey T. EBs recognize a nucleotide-dependent structural cap at growing microtubule ends. Cell. 2012; 149:371–382. [PubMed: 22500803]

Meijering E, Dzyubachyk O, Smal I. Methods for cell and particle tracking. Methods Enzymol. 2012; 504:183–200. [PubMed: 22264535]

Mulder AM, Glavis-Bloom A, Moores CA, Wagenbach M, Carragher B, Wordeman L, Milligan RA. A new model for binding of kinesin 13 to curved microtubule protofilaments. J Cell Biol. 2009; 185:51–57. [PubMed: 19332892]

Author Manuscript Author Manuscript Author Manuscript Author Manuscript

Neumann B, Hilliard MA. Loss of MEC-17 Leads to Microtubule Instability and Axonal Degeneration. Cell reports. 2014; 6:93–103. [PubMed: 24373971]

Nicastro D, Schwartz C, Pierson J, Gaudette R, Porter ME, McIntosh JR. The molecular architecture of axonemes revealed by cryoelectron tomography. Science. 2006; 313:944–948. [PubMed: 16917055]

Nogales E, Whittaker M, Milligan RA, Downing KH. High-resolution model of the microtubule. Cell. 1999; 96:79–88. [PubMed: 9989499]

Nogales E, Wolf SG, Downing KH. Structure of the alpha beta tubulin dimer by electron crystallography. Nature. 1998; 391:199–203. [PubMed: 9428769]

North BJ, Marshall BL, Borra MT, Denu JM, Verdin E. The human Sir2 ortholog, SIRT2, is an NAD +-dependent tubulin deacetylase. Mol Cell. 2003; 11:437–444. [PubMed: 12620231]

Odde D. Diffusion inside microtubules. European biophysics journal : EBJ. 1998; 27:514–520. [PubMed: 9760732]

Piperno G, Fuller MT. Monoclonal antibodies specific for an acetylated form of alpha-tubulin recognize the antigen in cilia and flagella from a variety of organisms. J Cell Biol. 1985; 101:2085–2094. [PubMed: 2415535]

Piperno G, LeDizet M, Chang XJ. Microtubules containing acetylated alpha-tubulin in mammalian cells in culture. J Cell Biol. 1987; 104:289–302. [PubMed: 2879846]

Poux AN, Cebrat M, Kim CM, Cole PA, Marmorstein R. Structure of the GCN5 histone acetyltransferase bound to a bisubstrate inhibitor. Proc Natl Acad Sci U S A. 2002; 99:14065–14070. [PubMed: 12391296]

Reed NA, Cai D, Blasius TL, Jih GT, Meyhofer E, Gaertig J, Verhey KJ. Microtubule acetylation promotes kinesin-1 binding and transport. Curr Biol. 2006; 16:2166–2172. [PubMed: 17084703]

Roll-Mecak A, Vale RD. Structural basis of microtubule severing by the hereditary spastic paraplegia protein spastin. Nature. 2008; 451:363–367. [PubMed: 18202664]

Schulze E, Asai DJ, Bulinski JC, Kirschner M. Posttranslational modification and microtubule stability. J Cell Biol. 1987; 105:2167–2177. [PubMed: 3316248]

Schulze E, Kirschner M. Dynamic and stable populations of microtubules in cells. J Cell Biol. 1987; 104:277–288. [PubMed: 3543024]

Shida T, Cueva JG, Xu Z, Goodman MB, Nachury MV. The major alpha-tubulin K40 acetyltransferase alphaTAT1 promotes rapid ciliogenesis and efficient mechanosensation. Proc Natl Acad Sci U S A. 2010; 107:21517–21522. [PubMed: 21068373]

Soppina V, Herbstman JF, Skiniotis G, Verhey KJ. Luminal localization of alpha-tubulin K40 acetylation by cryo-EM analysis of fab-labeled microtubules. PloS one. 2012; 7:e48204. [PubMed: 23110214]

Subramanian R, Ti SC, Tan L, Darst SA, Kapoor TM. Marking and measuring single microtubules by PRC1 and kinesin-4. Cell. 2013; 154:377–390. [PubMed: 23870126]

Sui H, Downing KH. Molecular architecture of axonemal microtubule doublets revealed by cryo-electron tomography. Nature. 2006; 442:475–478. [PubMed: 16738547]

Tahirovic S, Bradke F. Neuronal polarity. Cold Spring Harbor perspectives in biology. 2009; 1:a001644. [PubMed: 20066106]

Takemura R, Okabe S, Umeyama T, Kanai Y, Cowan NJ, Hirokawa N. Increased microtubule stability and alpha tubulin acetylation in cells transfected with microtubule-associated proteins MAP1B, MAP2 or tau. J Cell Sci. 1992; 103(Pt 4):953–964. [PubMed: 1487506]

Taschner M, Vetter M, Lorentzen E. Atomic resolution structure of human alpha-tubulin acetyltransferase bound to acetyl-CoA. Proc Natl Acad Sci U S A. 2012; 109:19649–19654. [PubMed: 23071318]

Topalidou I, Keller C, Kalebic N, Nguyen KC, Somhegyi H, Politi KA, Heppenstall P, Hall DH, Chalfie M. Genetically separable functions of the MEC-17 tubulin acetyltransferase affect microtubule organization. Curr Biol. 2012; 22:1057–1065. [PubMed: 22658602]

Varga V, Leduc C, Bormuth V, Diez S, Howard J. Kinesin-8 motors act cooperatively to mediate length-dependent microtubule depolymerization. Cell. 2009; 138:1174–1183. [PubMed: 19766569]

Author Manuscript Author Manuscript Author Manuscript Author Manuscript

von Hippel PH, Berg OG. Facilitated target location in biological systems. J Biol Chem. 1989; 264:675–678. [PubMed: 2642903]

Webster DR, Borisy GG. Microtubules are acetylated in domains that turn over slowly. J Cell Sci. 1989; 92(Pt 1):57–65. [PubMed: 2674164]

Wloga D, Gaertig J. Post-translational modifications of microtubules. J Cell Sci. 2010; 123:3447–3455. [PubMed: 20930140]

Xiao H, Verdier-Pinard P, Fernandez-Fuentes N, Burd B, Angeletti R, Fiser A, Horwitz SB, Orr GA. Insights into the mechanism of microtubule stabilization by Taxol. Proc Natl Acad Sci U S A. 2006; 103:10166–10173. [PubMed: 16801540]

Yajima H, Ogura T, Nitta R, Okada Y, Sato C, Hirokawa N. Conformational changes in tubulin in GMPCPP and GDP-taxol microtubules observed by cryoelectron microscopy. J Cell Biol. 2012; 198:315–322. [PubMed: 22851320]

Zhang Y, Ma C, Delohery T, Nasipak B, Foat BC, Bounoutas A, Bussemaker HJ, Kim SK, Chalfie M. Identification of genes expressed in C. elegans touch receptor neurons. Nature. 2002; 418:331–335. [PubMed: 12124626]

Ziolkowska NE, Roll-Mecak A. In vitro microtubule severing assays. Methods Mol Biol. 2013; 1046:323–334. [PubMed: 23868597]

Author Manuscript Author Manuscript Author Manuscript Author Manuscript

Highlights

1. TAT active site is not designed for efficient catalysis and proton transfer
2. TAT scans the microtubule bidirectionally and acetylates it stochastically
3. TAT catalytic rate, not substrate access is limiting for microtubule acetylation
4. TAT can function as an enzymatic timer for microtubule lifetimes

Author Manuscript Author Manuscript Author Manuscript Author Manuscript

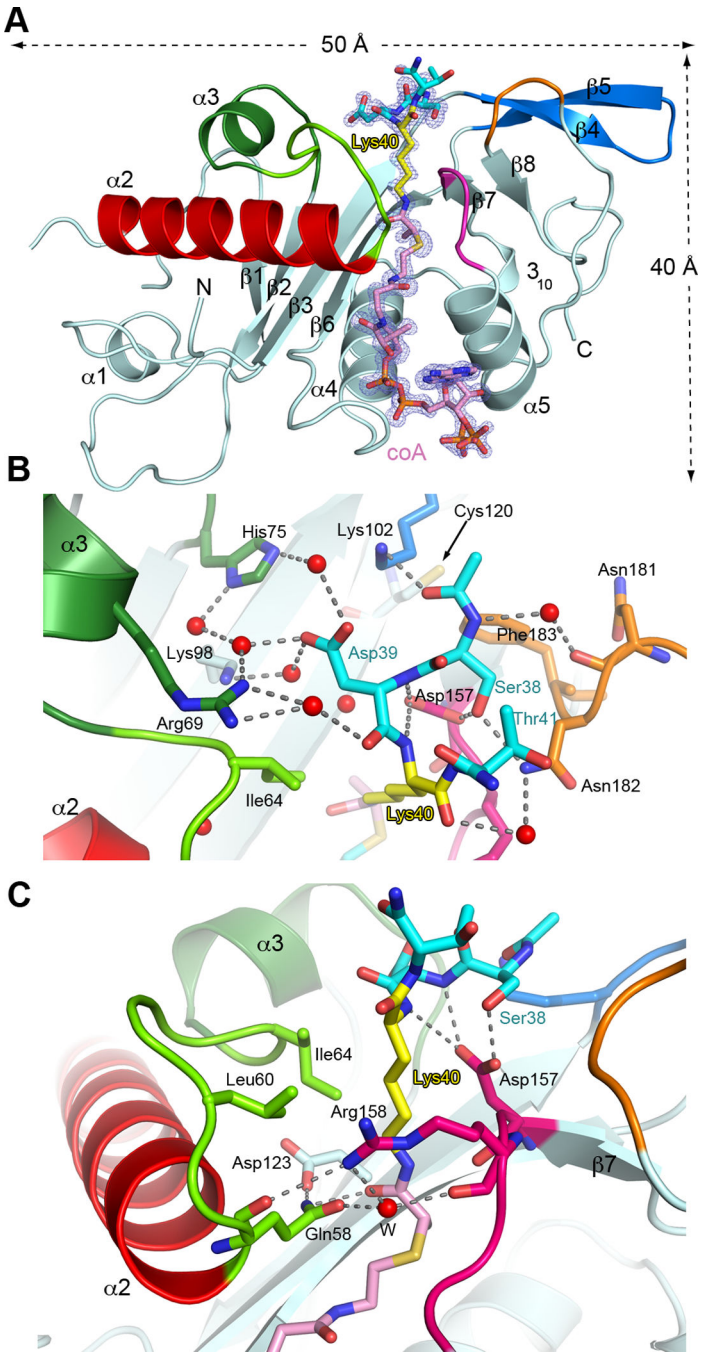

Figure 1.

Active site architecture and α−tubulin Lys40 loop recognition (A) Ribbon representation of TAT bound to peptide-coA bisubstrate analog 1 (IC50 ∼ 100 μM; Figures S1C and S1D); analog, shown as a stick model with Lys40 yellow, the rest of the peptide moiety, cyan, coA and linker, pink in the same scheme as Figure S1C; the $|F_o|$-$|F_c|$ density (prior to modeling the ligand) is contoured at 3.5σ (blue); Regions engaged in substrate binding and catalysis colored green, red, magenta, orange and blue (B) Close-up of the active site showing residues engaged in tubulin peptide recognition; red spheres and dashed lines denote water

molecules and hydrogen bonds, respectively; color scheme as in A; TAT residues labeled in black, peptide residues in color (C) Close-up of the active site showing residues important for Lys40 recognition and catalysis; colored as in A. Water molecule depicted as a red sphere labeled W. See also Figure S1 and Table S1.

Author Manuscript Author Manuscript Author Manuscript Author Manuscript

Author Manuscript Author Manuscript Author Manuscript Author Manuscript

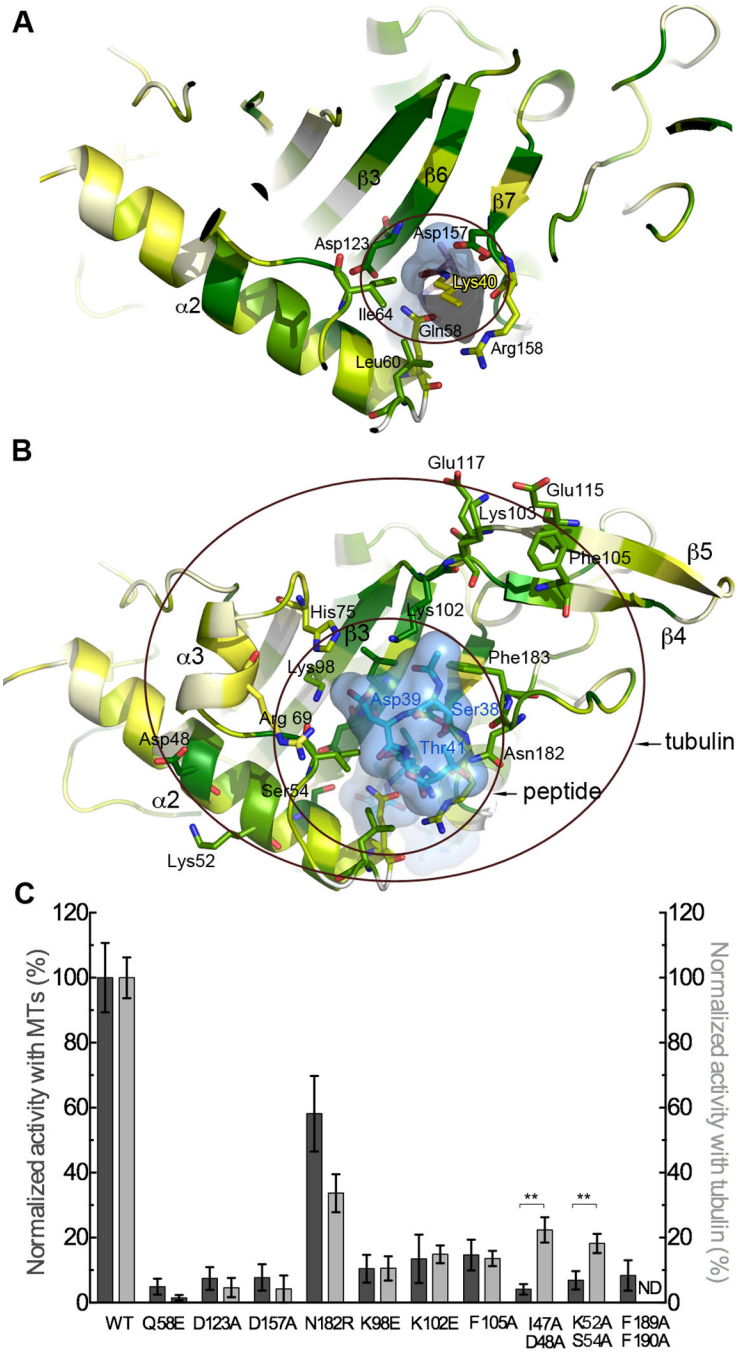

Figure 2.

Molecular determinants for Lys40 loop and tubulin recognition (A) A slice through TAT shown in ribbon representation color-coded for conservation on a gradient from white (40% identity) to green (100% identity). The tubulin peptide bisubstrate analog is shown as a stick model encased in a transparent molecular surface with α-tubulin Lys40 yellow (B) Peptide and tubulin binding interface. Inner and outer circles denote interaction surfaces with the Lys40 loop and tubulin, respectively. TAT represented as in A, TAT residues labeled in black, peptide residues in blue. The Lys40 side chain projects into the plane of the figure

and is not visible in this view. (C) Normalized acetylation activity of structure-guided TAT mutants with microtubules (dark grey) and tubulin (light grey). Error bars indicate standard error of the mean (S.E.M.; N≥3). **, $p < 0.01$, *t*-test. See also Figure S2.

Author Manuscript Author Manuscript Author Manuscript Author Manuscript

Author Manuscript Author Manuscript Author Manuscript Author Manuscript

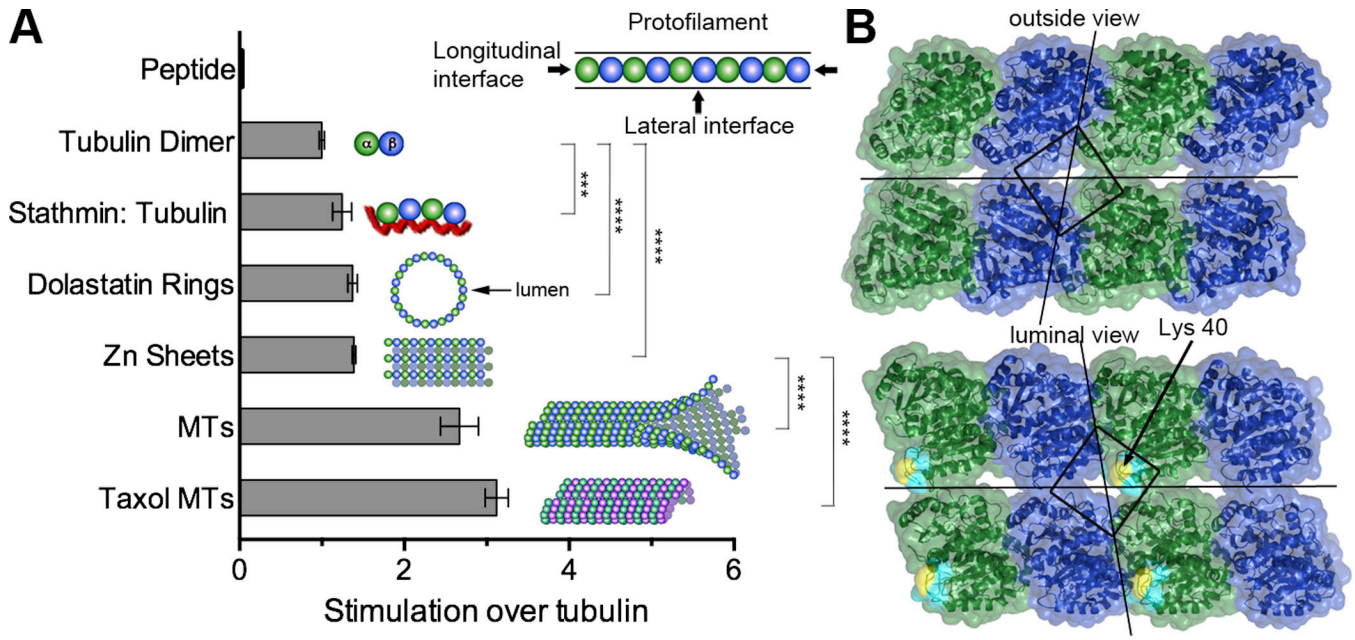

Figure 3.

TAT activity is enhanced predominantly by lateral lattice interactions (A) TAT activity with tubulin substrates of diverse geometries schematically represented with α-and β-tubulin as green and blue spheres, respectively. Stathmin, shown as red line. MTs, non-taxol stabilized glycerol microtubules; taxol MTs, microtubules stabilized with 20 μM taxol. The presence of dolastatin-10 rings, Zn sheets and microtubules under the reaction conditions was confirmed by negative stain EM (Figure S3A). Error bars indicate S.E.M. (N≥3). ***, $p < 0.001$, ****, $p < 0.0001$, *t*-test (B) Outer and luminal surface of two microtubule protofilaments; α-and β-tubulin, colored green and blue, respectively; the modeled Lys40 loop (visible only in the luminal view) is shown in cyan with Lys40 in yellow. Lines bisecting the surface indicate longitudinal and lateral microtubule lattice interfaces. The square surrounds the vertex of four tubulin subunits that overlies the Lys40 loop.

Author Manuscript Author Manuscript Author Manuscript Author Manuscript

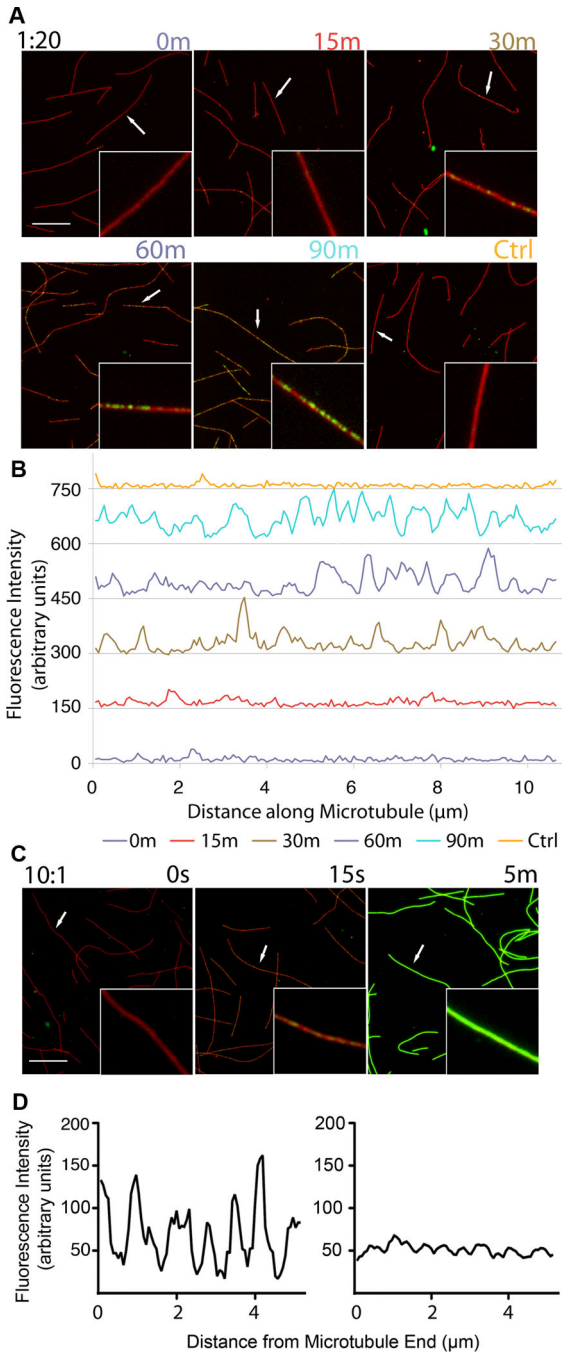

Figure 4.

Acetylation occurs stochastically along the microtubule and is not biased for microtubule ends (A) Time-course of taxol stabilized microtubules stained for tubulin (red) and acetylated tubulin (green) after exposure to TAT at 1:20 TAT: tubulin molar ratio; insets, close-ups of selected microtubules (arrows); scale bar 5 μm. (B) Line-scans of selected microtubules (arrows) from panel A in the acetylated tubulin channel. Line-scans from successive time points are staggered vertically by 150 units for clarity. (C) Time-course of taxol microtubules exposed to excess TAT at 10:1 TAT:tubulin molar ratio; insets, close-ups

of selected microtubules (arrows); scale bar 5 μm. (D) Analysis of acetylation near microtubule ends with excess TAT 15 seconds into the reaction. Left, representative scan of the terminal 5 μm of a microtubule; right, average of 25 line-scans of microtubule ends from the tip to 5μm into the microtubule. Scanned microtubules had 10 μm minimum length. See also Figure S4.

Author Manuscript Author Manuscript Author Manuscript Author Manuscript

Author Manuscript Author Manuscript Author Manuscript Author Manuscript

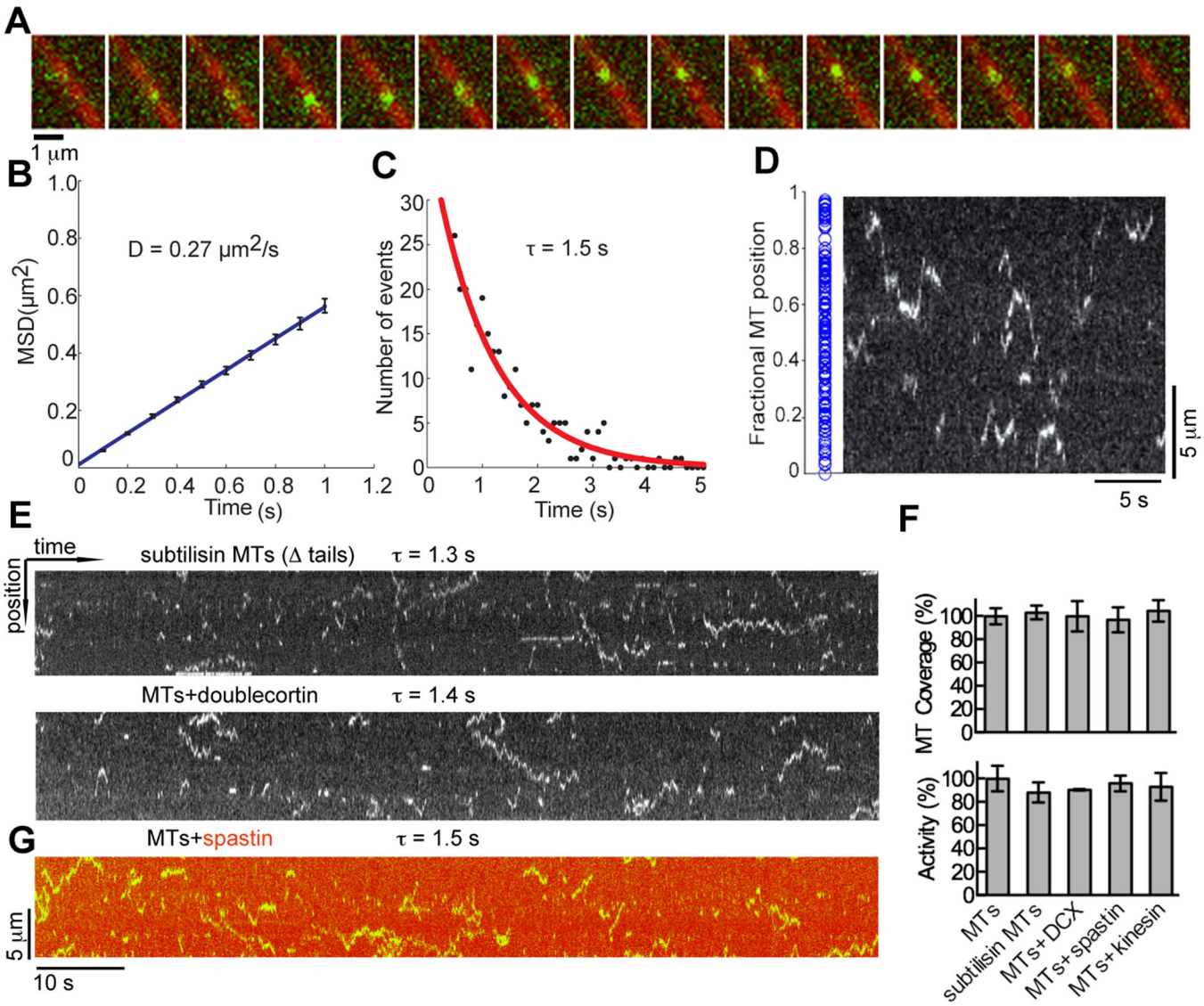

Figure 5.

TAT-GFP scans the microtubule (A) Sequential frames of a TAT-GFP (green) movie. 15 frames of a continuous TIRF recording (100 ms frames) were overlaid on one microtubule image (red). (B) Mean-squared displacement (MSD) of TAT-GFP plotted against time. A linear curve fitted to the shown time interval yields a diffusion coefficient of 0.27 ± 0.01 $\mu m^2/s$. Error bars represent S.E.M. (C) Distribution of durations of TAT-GFP interactions with the microtubule. An exponential curve fitted to the histogram and corrected for photobleaching (Figure S5A) yields a mean lifetime of interaction (τ) of 1.5 ± 0.3 s (R^2 = 0.91; N=269). (D) Initial positions (blue dots) of scanning TAT-GFP along microtubules, N=163 (left) (Figure S5C); kymograph depicting TAT-GFP motion on a microtubule showing random initial positions along the microtubule (right). (E) Kymographs depicting the motion of TAT-GFP on a subtilisin treated microtubule missing C-terminal tails (top) and microtubule in the presence of saturating amounts of doublecortin (bottom) (see also Figure S5K). (F) Normalized total microtubule length scanned by TAT-GFP molecules (top)

Author Manuscript Author Manuscript Author Manuscript Author Manuscript

and acetylation activity (bottom) with subtilisin microtubules and microtubules coated with doublecortin, spastin and kinesin-5 motor domain (see also Figure S5J). (G) Kymograph depicting the motion of TAT-GFP on microtubules decorated with DyLight 550 labeled spastin in the presence of ATPγS, which inhibits severing, but not microtubule binding (Roll-Mecak and Vale, 2008). τ, defined as in C.

Author Manuscript Author Manuscript Author Manuscript Author Manuscript

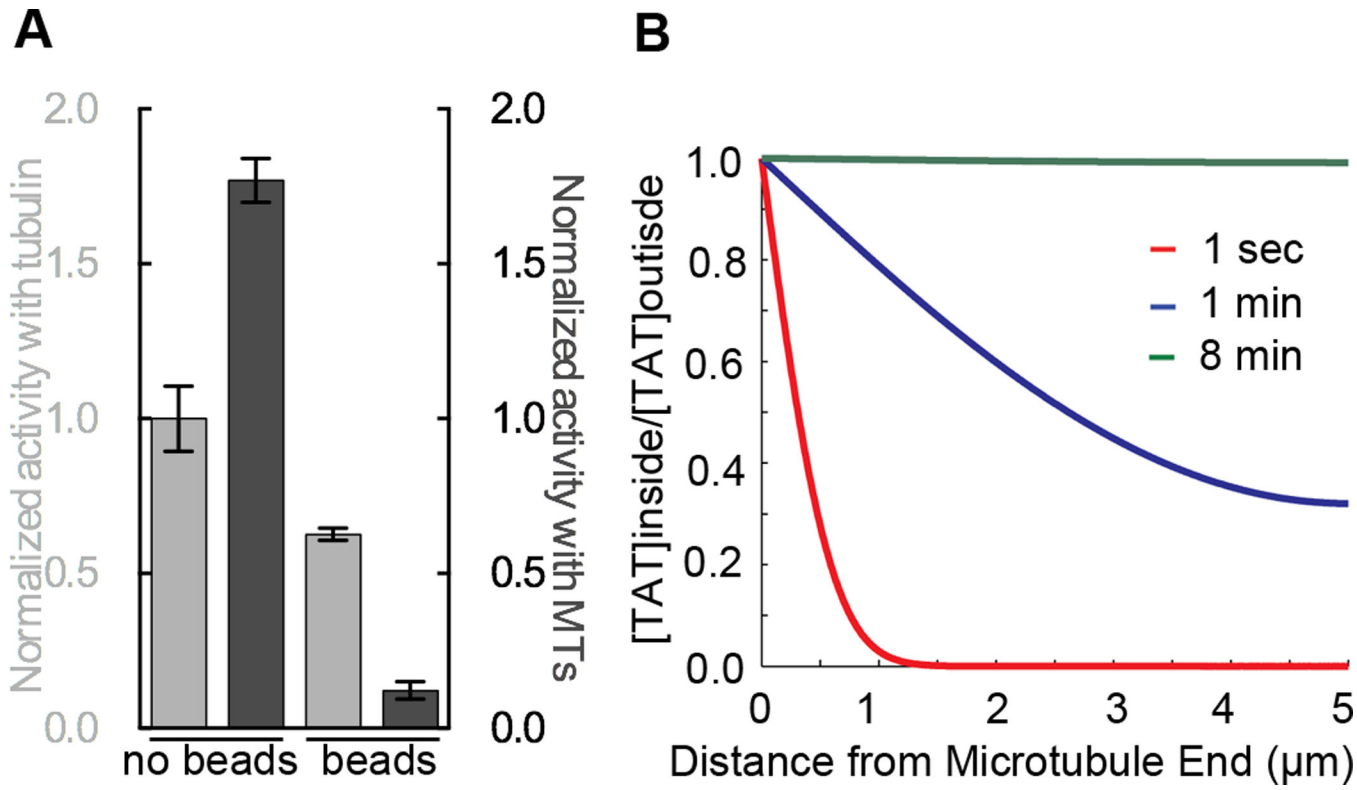

Figure 6.

Substrate access by TAT is spatially constrained but not rate limiting for microtubule acetylation (A) Normalized activity of biotinylated TAT, free in solution or immobilized to 1 μm diameter streptavidin beads, with tubulin (light grey) and microtubules (dark grey). (B) Calculated profiles of TAT diffusion into a microtubule (or probability of residence) at positions along the microtubule at indicated time points (Extended Experimental Procedures). At 8 min, TAT is completely equilibrated between the lumen of a 10 μm long microtubule and the outside volume. See also Figure S6.